JACS
JOURNAL OF THE AMERICAN CHEMICAL SOCIETY
pubs.acs.org/JACS
Article

Ions Speciation at the Water–Air Interface

Takakazu Seki,[#] Chun-Chieh Yu,[#] Kuo-Yang Chiang, Alessandro Greco, Xiaoqing Yu, Fumiki Matsumura, Mischa Bonn,* and Yuki Nagata*

Cite This: J. Am. Chem. Soc. 2023, 145, 10622–10630
Read Online
ACCESS | Metrics & More | Article Recommendations | Supporting Information

ABSTRACT: In typical aqueous systems, including naturally occurring sweet and salt water and tap water, multiple ion species are co-solvated. At the water–air interface, these ions are known to affect the chemical reactivity, aerosol formation, climate, and water odor. Yet, the composition of ions at the water interface has remained enigmatic. Here, using surface-specific heterodyne-detected sum-frequency generation spectroscopy, we quantify the relative surface activity of two co-solvated ions in solution. We find that more hydrophobic ions are speciated to the interface due to the hydrophilic ions. Quantitative analysis shows that the interfacial hydrophobic ion population increases with decreasing interfacial hydrophilic ion population at the interface. Simulations show that the solvation energy difference between the ions and the intrinsic surface propensity of ions determine the extent of an ion's speciation by other ions. This mechanism provides a unified view of the speciation of monatomic and polyatomic ions at electrolyte solution interfaces.

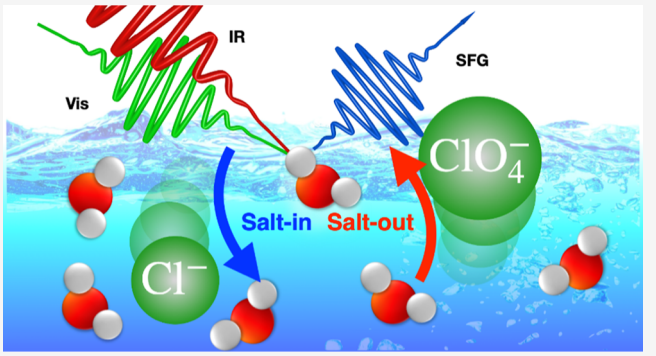

INTRODUCTION

Surface propensities of ions and ionic molecules at the water–air interface play a pivotal role in aerosol growth,[1] atmospheric chemistry,[2] and on-water chemistry.[3,4] At the water–air interface, the density of water is reduced, affecting both the level of ion hydration and the screening of charges through the locally reduced dielectric function[5] compared with the bulk. Both factors affect the surface propensity of ions. Molecular dynamics (MD) simulations,[6−12] as well as surface-specific measurements,[13−20] have revealed that the surface propensity of ions is linked with the Hofmeister series: ions that salt out proteins have stronger hydration and a correspondingly lower surface propensity.

The studies mentioned above have focused on solutions containing a single salt species. On the other hand, a vast majority of ion solutions in the world contain multiple species of salt and ions. For example, seawater contains a variety of inorganic ions such as Na^+, Cl^-, and Mg^{2+}, together with a very small amount of organic material, including ions. This tiny amount of organic material is believed to be salted out to the sea surface, affecting chemical and physical processes such as sea-spray aerosol[21] and algal bloom.[22] However, the distribution of such species at the water–air interface is poorly understood.[23] The following is a typical question: Can the surface propensity of organic ions be affected by other co-solvated ions? Answering this question allows us to resolve fundamental questions about water on earth; i.e., what is the consequence of the complex ion composition of seawater, and why can unexpectedly large iodine quantities be emitted from the sea surface?[24]

While the complexities of competitive ion adsorption have been investigated,[25−30] the experimental techniques often have difficulties disentangling the bulk contribution from the surface contribution.[27,29] Surface-specific spectroscopy such as sum-frequency generation (SFG) spectroscopy can probe the interfacial region selectively and thus has been used for investigating the cooperative ion adsorption at the water–polymer,[26] water–oil,[25] and water–surfactant[31,32] interfaces. However, the technique used in these studies is conventional SFG,[25,26,31,32] which prohibits us from quantifying the ions' propensity due to the cooperative behavior of multiple ions because the observables in the conventional SFG can interfere and are not simply additive.[33]

Here, we measure the O–D stretch mode of heavy water D_2O at the electrolyte solution–air interfaces with the surface-specific heterodyne-detected SFG (HD-SFG) technique[33−36] by mixing two different species of salts in D_2O. Thanks to the additivity of $\chi^{(2)}$ measured with HD-SFG, we can identify the impact of the salt on the interfaces quantitatively. Our data for various ion combinations show that hydrophobic ions, defined

Received: January 14, 2023
Published: May 4, 2023

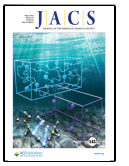

https://doi.org/10.1021/jacs.3c00517
J. Am. Chem. Soc. 2023, 145, 10622–10630

here as ions with a relatively low charge density and associated low solvation energy, are readily speciated (salted out) and are enriched at the interface by decreasing the population of interfacial hydrophilic ions with high charge density and solvation energy. As such, for electrolyte mixtures, ion distributions at the interfaces are determined by cooperative effects. Time-resolved SFG (TR-SFG) spectroscopy is used for probing the ion species that HD-SFG cannot probe. These data further support our notion that hydrophilic ions speciate the hydrophobic ones. MD simulations with two model ion species show that the hydrophobic ions are enriched when the solvation energy difference between hydrophobic and hydrophilic ions becomes large. This study highlights that the surface propensities of ions are significantly controlled by the surface propensity and bulk concentration of other co-existing ions.

RESULTS

SFG Signatures of Ions at the Water−Air Interface. For the HD-SFG measurements, we focused the infrared (IR) and visible beams collinearly onto a *y*-cut quartz to generate a local oscillator (LO) signal. A $SrTiO_3$ (STO) plate was inserted into the beam path to generate the delay for the LO beam relative to the other beams. These beams were refocused onto the electrolyte aqueous solutions−vapor interface. The angles of incidence were set to 45°. For the SFG measurement in this work, we used ssp polarization combination, where ssp denotes s-polarized SFG, s-polarized visible, and p-polarized IR beams. NaI solutions were freshly prepared just before the SFG measurements to avoid the oxidization of the iodide ion.[17] The details of the HD-SFG setup are presented in ref 37.

First, we measured the imaginary part of the SFG susceptibility (Im $\chi^{(2)}$) of the neat D_2O as well as the D_2O solution of 3.0 M NaSCN, 1.5 M $NaClO_4$, 1.5 M NaI, 3.0 M NaCl, 0.5 M Na_2SO_4, and 20 mM $NaBPh_4$ (chemical structures are shown in Figure 1a) at the solution−vapor interfaces. The data are displayed in Figure 1b. The O−D stretch mode region for the neat D_2O spectrum (Im $\chi^{(2)}_{D_2O}$) shows the 2730 cm^{-1} positive peak, 2650 cm^{-1} positive shoulder peak, and 2550 cm^{-1} negative band, consistent with previous reports,[38,39] arising from the dangling (free) O−D group, the anti-symmetric mode of the D_2O molecules with two hydrogen-bond donors, and the hydrogen-bonded O−D group, respectively.[40,41] The addition of salts in the neat D_2O alters the Im $\chi^{(2)}$ spectral features drastically; NaSCN, $NaClO_4$, NaI, and $NaBPh_4$ make the <~2500 cm^{-1} Im $\chi^{(2)}$ features positive. NaCl (Na_2SO_4) elevates (lowers) the <2550 cm^{-1} Im $\chi^{(2)}$ negative features. Furthermore, NaSCN, NaI, and $NaClO_4$ ions reduce the free O−D feature, and $NaBPh_4$ ions completely suppress it. These features are qualitatively consistent with several previous reports,[42,43] although some details (e.g., for NaCl and $NaClO_4$) are different,[43,44] possibly because of the phase inaccuracy of the previous HD-SFG measurement, as pointed out in ref 45. To our knowledge, no HD-SFG data for $NaBPh_4$ have been published previously.

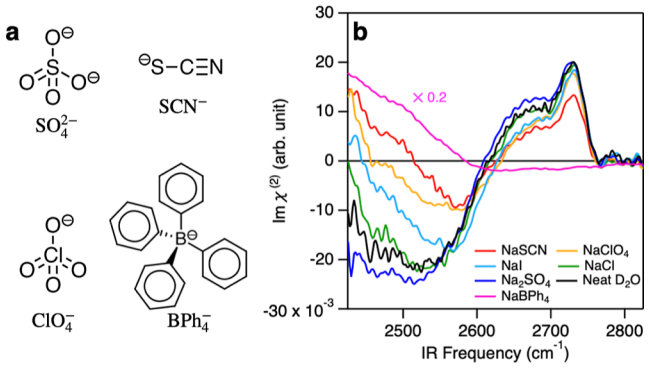

Figure 1. (a) Chemical structures of SO_4^{2-}, SCN^-, ClO_4^-, and BPh_4^- anions. (b) Im $\chi^{(2)}$ spectra of the neat D_2O as well as the D_2O solution of 3.0 M NaSCN, 1.5 M $NaClO_4$, 1.5 M NaI, 3.0 M NaCl, 0.5 M Na_2SO_4, and 20 mM $NaBPh_4$ at the solution−vapor interfaces. For clarity, the Im $\chi^{(2)}$ spectrum for $NaBPh_4$ was scaled by a factor of 0.2.

The amplitudes of the Im $\chi^{(2)}$ spectra in the hydrogen-bonded O−D stretch region (for example, at 2500 cm^{-1}) show the trend that the amplitude is large in the order $BPh_4^- > SCN^- > ClO_4^- > I^- > Cl^- > SO_4^{2-}$. This inversely follows the Hofmeister series $BPh_4^- < SCN^- < ClO_4^- < I^- < Cl^- < SO_4^{2-}$,[46,47] which represents the rank for speciation ability. Because the larger Im $\chi^{(2)}$ amplitude in the hydrogen-bonded O−D region indicates the higher surface propensity of ions, the data show that the surface propensity of the ions is linked with the Hofmeister series, as is pointed out theoretically[48] and experimentally.[43]

Composition of Ions at Ion Co-solvated Solution Interfaces. Next, we focused on the Im $\chi^{(2)}$ spectra for the electrolyte mixtures. We prepared solutions of 0.75 M $NaClO_4$/0.75 M NaCl, 0.75 M NaI/0.75 M NaCl, 1.5 M NaSCN/1.5 M NaCl, 0.25 M Na_2SO_4/0.5 M NaCl, and 10 mM $NaBPh_4$/10 mM NaCl and obtained the Im $\chi^{(2)}$ spectra at these solution−vapor interfaces (denoted as Im $\chi^{(2)}_{ClO_4^-/Cl^-}$, Im $\chi^{(2)}_{I^-/Cl^-}$, Im $\chi^{(2)}_{SCN^-/Cl^-}$, Im $\chi^{(2)}_{SO_4^{2-}/Cl^-}$, and Im $\chi^{(2)}_{BPh_4^-/Cl^-}$, respectively). Figure 2a displays the Im $\chi^{(2)}_{ClO_4^-/Cl^-}$ spectrum, showing a spectral feature similar to the Im $\chi^{(2)}$ spectrum of the 1.5 M $NaClO_4$ solution (Im $\chi^{(2)}_{ClO_4^-}$) but different from the Im $\chi^{(2)}$ spectrum of the 1.5 M NaCl solution (Im $\chi^{(2)}_{Cl^-}$). Apparently, the Im $\chi^{(2)}_{ClO_4^-/Cl^-}$ spectrum is not the weighted average of the Im $\chi^{(2)}_{ClO_4^-}$ and Im $\chi^{(2)}_{Cl^-}$ spectra. This indicates that the composition of anions at the interface is not 50% ClO_4^- and 50% Cl^-; rather, the interfacial region is more heavily populated by ClO_4^- ions. This suggests that the more hydrophobic ClO_4^- ion is speciated at the water−vapor interface by the co-solvated hydrophilic Cl^- ion.

To evaluate the interfacial composition of ions, we computed the coefficient $c_{ClO_4^-}$ and c_{Cl^-} by assuming that Im $\chi^{(2)}_{ClO_4^-/Cl^-}$ can be described by a linear combination of the Im $\chi^{(2)}_{ClO_4^-}$ and Im $\chi^{(2)}_{Cl^-}$ spectra; i.e., one ion will be replaced by the other ion at the interfaces

$$\text{Im}\,\chi^{(2)}_{ClO_4^-/Cl^-} = c_{ClO_4^-}\text{Im}\,\chi^{(2)}_{ClO_4^-} + c_{Cl^-}\text{Im}\,\chi^{(2)}_{Cl^-} \quad (1)$$

where we assume that $c_{ClO_4^-} + c_{Cl^-} = 1$. Note that the validation of this assumption is confirmed in the simulation (see the Supporting Information, Figure S3). The fit result is given in Figure 2a with the coefficients of ($c_{ClO_4^-}$, c_{Cl^-}) = (0.62 ± 0.02, 0.38 ± 0.02), indicating that the D_2O−vapor interface is dominated by ClO_4^- and the concentration of Cl^- decreases.

https://doi.org/10.1021/jacs.3c00517
J. Am. Chem. Soc. 2023, 145, 10622−10630

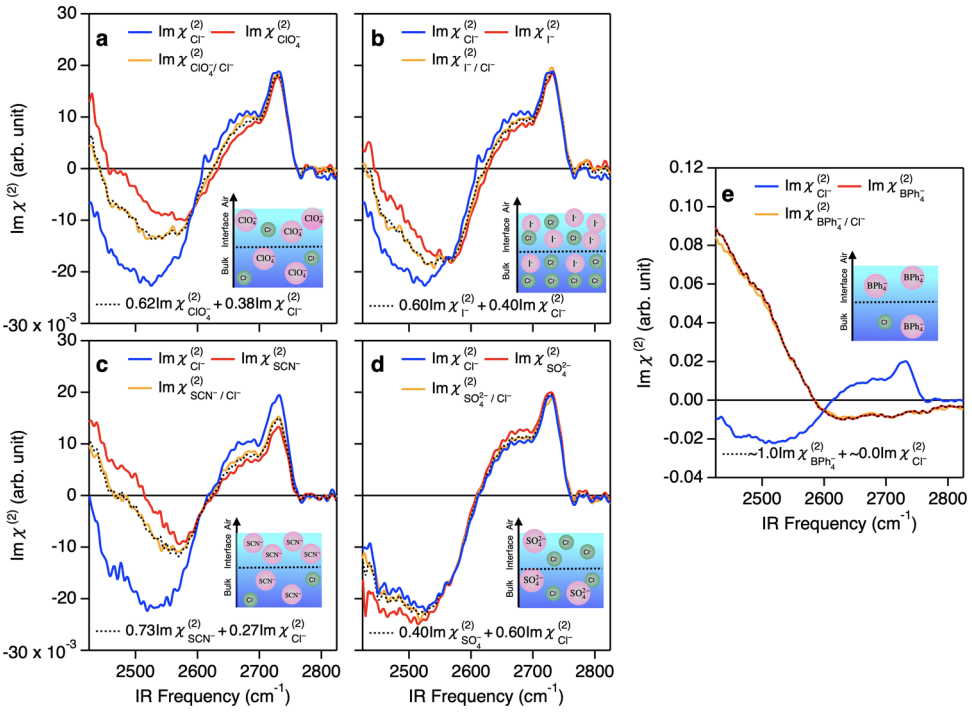

Figure 2. (a–e) Im $\chi^{(2)}$ spectra at the D_2O–vapor interfaces with various salt mixtures: (a) 1.5 M NaCl ($\chi^{(2)}_{Cl^-}$), 1.5 M $NaClO_4$ ($\chi^{(2)}_{ClO_4^-}$), and 0.75 M $NaClO_4$ + 0.75 M NaCl ($\chi^{(2)}_{ClO_4^-/Cl^-}$); (b) 1.5 M NaCl ($\chi^{(2)}_{Cl^-}$), 1.5 M NaI ($\chi^{(2)}_{I^-}$), and 0.75 M NaI + 0.75 M NaCl ($\chi^{(2)}_{I^-/Cl^-}$); (c) 3.0 M NaCl ($\chi^{(2)}_{Cl^-}$), 3.0 M NaSCN ($\chi^{(2)}_{SCN^-}$), and 1.5 M NaSCN + 1.5 M NaCl ($\chi^{(2)}_{SCN^-/Cl^-}$); (d) 1.0 M NaCl ($\chi^{(2)}_{Cl^-}$), 0.5 M Na_2SO_4 ($\chi^{(2)}_{SO_4^{2-}}$), and 0.25 M Na_2SO_4 + 0.5 M NaCl ($\chi^{(2)}_{SO_4^{2-}/Cl^-}$); (e) 20 mM NaCl ($\chi^{(2)}_{Cl^-}$), 20 mM $NaBPh_4$ ($\chi^{(2)}_{BPh_4^-}$), and 10 mM $NaBPh_4$ + 10 mM NaCl ($\chi^{(2)}_{BPh_4^-/Cl^-}$). The black dotted lines represent the fits based on eq 1. The inset schematics depict the putative picture of interfacial ions' distribution.

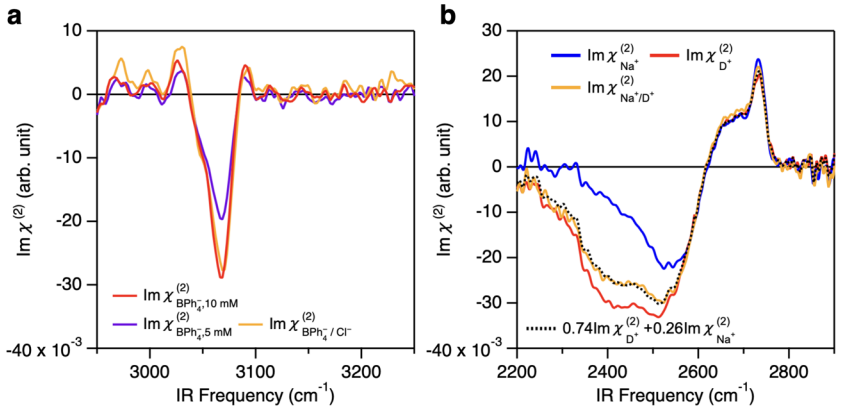

Figure 3. (a,b) HD-SFG measurement of $NaBPh_4$ and DCl with NaCl at the D_2O–vapor interfaces: (a) 5 mM $NaBPh_4$ + 5 mM NaCl ($\chi^{(2)}_{BPh_4^-/Cl^-}$) and 5 and 10 mM $NaBPh_4$ ($\chi^{(2)}_{BPh_4^-,5mM}$ and $\chi^{(2)}_{BPh_4^-,10mM}$, respectively). (b) 1.0 M NaCl ($\chi^{(2)}_{Na+}$), 1.0 M DCl ($\chi^{(2)}_{D+}$), and 0.5 M DCl + 0.5 M NaCl ($\chi^{(2)}_{Na+/D+}$). The black dotted lines represent the fits based on eq 1.

Subsequently, we performed the same analysis for the other electrolyte combinations. Figure 2b–d displays the Im $\chi^{(2)}_{I^-/Cl^-}$, Im $\chi^{(2)}_{SCN^-/Cl^-}$, Im $\chi^{(2)}_{SO_4^{2-}/Cl^-}$, and Im $\chi^{(2)}_{BPh_4^-/Cl^-}$ spectra. The fits using eq 1 provide (c_{I^-}, c_{Cl^-}) = (0.60 ± 0.02, 0.40 ± 0.02), (c_{SCN^-}, c_{Cl^-}) = (0.73 ± 0.02, 0.27 ± 0.02), ($c_{SO_4^{2-}}$, c_{Cl^-}) = (0.40 ± 0.06, 0.60 ± 0.06), and ($c_{BPh_4^-}$, c_{Cl^-}) = (1.00 ± 0.02, 0.00 ± 0.02), where the error bars were estimated from the fits. For the fittings of Im $\chi^{(2)}_{SCN^-/Cl^-}$, Im $\chi^{(2)}_{SO_4^{2-}/Cl^-}$, and Im $\chi^{(2)}_{BPh_4^-/Cl^-}$, we used the Im $\chi^{(2)}$ spectra of the 3.0 M, 1.0 M, and 20 mM NaCl solutions for Im $\chi^{(2)}_{Cl^-}$ to have the same concentration of salt, respectively. The relative strength of the coefficients c is in the order $c_{BPh_4^-} > c_{SCN^-} > c_{ClO_4^-} > c_{I^-} > c_{Cl^-} > c_{SO_4^{2-}}$. This means that not only the surface propensity but also the amount of the speciation of ions in the co-solvated solutions is governed by the Hofmeister series; hydrophobic ions tend to be speciated at the water–air interface due to the presence of the hydrophilic ions. The amount of enhancement of the surface hydrophobic ion concentration is compensated by the amount

https://doi.org/10.1021/jacs.3c00517
J. Am. Chem. Soc. 2023, 145, 10622–10630

of decreases in the surface hydrophilic ion concentration; however, it is at a maximum 50% among the anions considered in the Hofmeister series, i.e., except BPh_4^-. Note that for ion speciation, nuclear quantum effects are negligible, as is evidenced by the same coefficients obtained in H_2O solutions (see Supporting Information).

Direct Probe of the Anion and Cation. The above O−D stretch data infer the speciation of hydrophobic anions from changes in the water response, but this does not probe the anion itself directly. To capture the speciation of the anion at the interface, we focused on the BPh_4^- anion and probed the aromatic C−H stretch mode of BPh_4^- at ∼3065 cm^{-1} (Figure 1a);[49,50] Figure 3 displays Im $\chi^{(2)}$ spectra of 5 mM $NaBPh_4$/5 mM NaCl co-solvated D_2O solution ($\chi^{(2)}_{BPh_4^-/Cl-}$) together with 5 and 10 mM $NaBPh_4$ D_2O solutions ($\chi^{(2)}_{BPh_4^-,5mM}$ and $\chi^{(2)}_{BPh_4^-,10mM}$) in the aromatic C−H stretch region. These Im $\chi^{(2)}$ spectra show a sharp negative peak at ∼3065 cm^{-1} only as there is no resonance for D_2O. The increase in the concentration of BPh_4^- enhances the amplitude of the C−H peak for the pure $NaBPh_4$ solutions. Remarkably, the 5 mM $NaBPh_4$/5 mM NaCl co-solvated solution shows the same amplitude of the C−H stretch feature as the 10 mM $NaBPh_4$ solution. These data confirm that the hydrophobic ions are enriched substantially due to the chloride ion-induced speciation.

To examine whether this speciation occurs not only for anions but also for cations, we measured the SFG spectra of the mixture of 0.5 M NaCl/0.5 M DCl (Im $\chi^{(2)}_{Na+/D+}$), 1.0 M NaCl (Im $\chi^{(2)}_{Na+}$), and 1.0 M DCl solutions (Im $\chi^{(2)}_{D+}$). Because D_3O^+ is known to be surface active and generates an SFG proton continuum response in the frequency region below the O−D stretch region,[51,52] one can probe interfacial D_3O^+ directly. The data are shown in Figure 3b. The Im $\chi^{(2)}_{D+}$ spectrum and the Im $\chi^{(2)}_{Na+/D+}$ spectrum show the D_3O^+ feature in the frequency <2300 cm^{-1}. The analysis for the linear combination of the spectra gives coefficients of (c_{D^+}, c_{Na^+}) = (0.74 ± 0.02, 0.26 ± 0.02), clearly demonstrating that in the interfacial region, D_3O^+ is disproportionally enriched compared with the bulk due to the presence of Na^+. This observation manifests that the speciation effect occurs regardless of the sign of the ionic charge.

Above, we showed that the D_3O^+ signature is dominant for the Im $\chi^{(2)}_{Na+/D+}$ spectrum, while the Na^+ signature is not clearly present, and thus, it remains unclear whether a large amount of Na^+ is depleted from the interfacial region. To probe the Na^+ signature, we carried out the TR-SFG measurement with homodyne detection. Hsieh et al. reported long-lived oscillations (∼1 ns) in time-resolved IR pump/SFG probe signals for different ion solutions,[53] after the excess vibrational energy is fully relaxed (∼1 ps). This oscillation was assigned to the interference between the SFG signals generated at the water−air interface and that at the shock wave front. The period of the oscillation is the same for different ion solutions since the propagation of the shock wave front is determined by the speed of sounds, which is nearly constant. In contrast, the amplitude and phase of the oscillation differ significantly between different ion solutions. Thus, the long-lived oscillation serves as a reporter of the ion composition at the interface.

Figure 4 shows the time evolutions of the integrated SFG intensities ($I(t)$) of the 0.5 M DCl + 0.5 M NaCl solution,

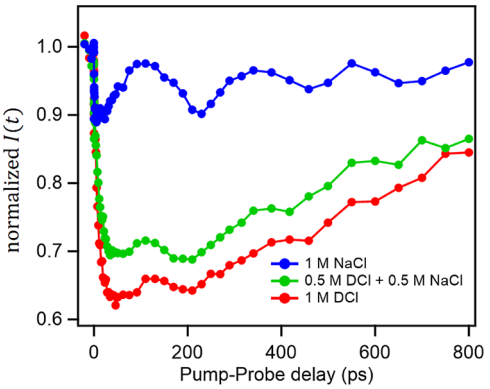

Figure 4. TR-SFG time trace signals of DCl with NaCl at the D_2O−vapor interfaces. The samples are 1.0 M NaCl, 1.0 M DCl, and 0.5 M DCl + 0.5 M NaCl solutions. The 1.0 M NaCl sample shows strong GHz oscillations, reduced in the presence of excess hydrated protons.

together with the traces of 1.0 M DCl and 1.0 M NaCl solutions, measured at the water−solution interfaces. The samples used in the TR-SFG data are the same as those used for the measurement of Figure 3b. The pure DCl and NaCl solutions exhibit the characteristic dynamics; the NaCl solution shows the characteristic time trace with a large oscillation,[53] while DCl does not. The mixture solution of 0.5 M DCl + 0.5 M NaCl exhibits a very small oscillation, compared with the pure 1 M NaCl sample. This small oscillation manifests that Na^+ is excluded from the interfacial region. Note that since the TR-SFG measurement was performed using homodyne detection, so the different signals do not simply add up, prohibiting us from obtaining the coefficients like eq 1. Yet it is apparent from the data that these are consistent with the signal from the DCl/NaCl mixture being dominated by that of the pure DCl response.

DISCUSSION

To generalize the idea of the speciation of ions, we simulated the system of the two model salts, NaX and NaY, dissolved in a water solution (∼1.2 M for each anion). X^- and Y^- have the same Lennard−Jones (LJ) energy minima, while the radii of the LJ potential differ between X^- and Y^-. We set X^- to have the larger radius (σ_{X^-}) than the radius of Y^- (σ_{Y^-}), making X^- more hydrophobic than Y^- in the spirits of refs 54 and 55. σ_{X^-} and σ_{Y^-} were set by multiplying a factor to the Cl^- radius (σ_{Cl^-}), while we used the Na^+ radius for the cation without scaling (see more details in the Supporting Information).[56] As a reference, we simulated the pure ∼2.4 M NaX solution, where the concentration of NaX equals the sum of the concentrations of NaX and NaY in the co-solvated solutions. We first fixed σ_{X^-} and changed σ_{Y^-}. The depth profiles of the X^- concentrations are shown in Figure 5a,b for the cases of $\sigma_{X^-} = 1.10\sigma_{Cl^-}$ and $1.05\sigma_{Cl^-}$, respectively. The depth axis is denoted as z, and the origin point of the z axis is the position of the Gibbs dividing surface (GDS) of water.

First, we discuss the case of $\sigma_{X^-} = 1.10\sigma_{Cl^-}$ (Figure 5a). The comparison between the pure NaX solution and NaX/NaY co-solvated solutions in the bulk region ($z < -10$ Å) shows that the bulk concentration of X^- in the co-solvated solution is

https://doi.org/10.1021/jacs.3c00517
J. Am. Chem. Soc. 2023, 145, 10622−10630

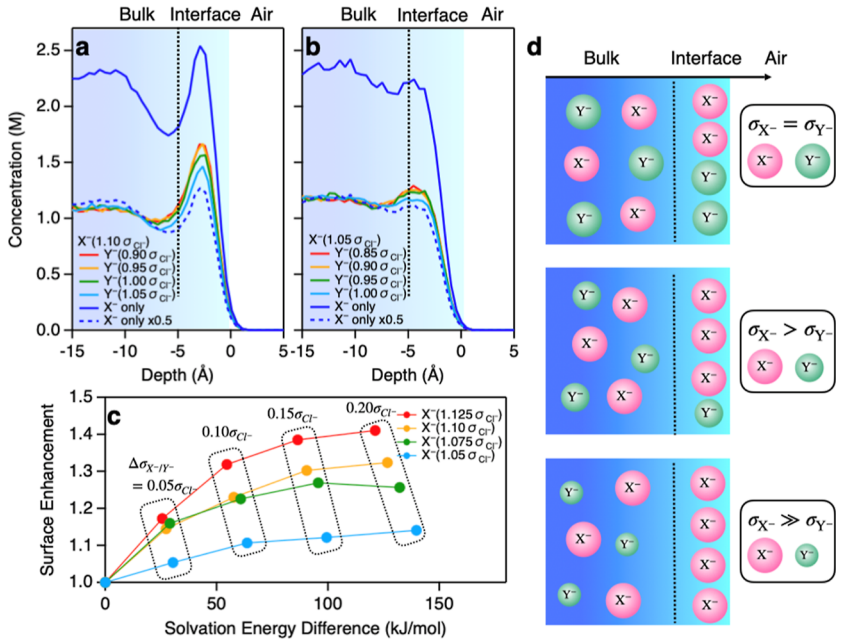

Figure 5. (a,b) Depth profiles of the X^- concentration (bulk concentrations: ∼2.4 M for pure NaX and ∼1.2 M each for co-solvated NaX/NaY solutions). $z = 0$ represents the position of the GDS of water. The LJ radii of X^- are (a) $1.10\sigma_{Cl^-}$ and (b) $1.05\ \sigma_{Cl^-}$. The boundary of the interfacial region and bulk is defined as 5 Å below GDS. (c) Surface enrichment of anion as a function of the solvation energy difference of X^- and Y^-. The surface enrichment is defined as the relative peak concentration in the range $-2.4\ Å < z < 4.4\ Å$ region for X^- in mixture solutions with respect to those for pure X^- in the blue dotted lines. The peak positions and concentrations were determined based on quadratic fits. $\sigma_{X^-} - \sigma_{Y^-} \equiv \Delta\sigma_{X^-/Y^-}$. With increasing $\Delta\sigma_{X^-/Y^-}$, the surface enhancement becomes more prominent. Note that the error bars in panels (a−c) are negligibly small (see the Supporting Information). (d) Schematic of the speciation of ions with the variation of LJ radii of ions.

nearly half of that in the pure solution. In contrast, at the interface ($5\ Å > z > -5\ Å$), the concentrations of X^- in the co-solvated solutions are larger than half of the X^- concentration in the pure solution. This confirms that the hydrophobic anion is speciated. The interfacial X^- concentration increases with increasing difference between the X^- and Y^- radii, indicating that X^- is more salted out and Y^- is more salted in (see also the depth profiles for Y^- ion in the Supporting Information). The solvation energy difference of X^- and Y^- is sizable at 58 kJ/mol when $(\sigma_{X^-}, \sigma_{Y^-}) = (1.10\sigma_{Cl^-}, 1.00\sigma_{Cl^-})$, similar to the solvation energy difference between I^- and Cl^- of 63 kJ/mol. In this case, the simulation suggests that the peak concentration of X^- in the 1.2 M NaX/1.2 M NaY co-solvated solution is 124% of the half of that in the 2.4 M NaX solution at the solution−air interfaces. This inferred surface enrichment is consistent with the interface concentration of $(c_{I^-}, c_{Cl^-}) = (0.60 \pm 0.02, 0.40 \pm 0.02)$ concluded from the SFG spectra (Figure 2b). This quantitative agreement between the SFG data and simulation manifests that the surface enhancement of the ion occurs because of the difference in the hydrophobicity of the ions.

When looking at the case of $\sigma_{X^-} = 1.05\sigma_{Cl^-}$ (Figure 5b), one notices that the concentration of X^- shows less interfacial accumulation. This is because X^- becomes less hydrophobic, the surface propensity of X^- is thus rather low, and the surface enrichment is limited. These observations are summarized in Figure 5c,d, where the surface enrichment of X^- is plotted as a function of the solvation energy difference of X^- and Y^- anions. Overall, the surface propensity of X^- is enhanced with increasing solvation energy difference between X^- and Y^-, but this is not the only factor in determining the surface enrichment of X^-. The other key factor is the hydrophobicity of X^-; if X^- is more hydrophobic, X^- will be more surface active, as demonstrated by several past pioneering works.[57,58] This clearly demonstrates that the extent of the speciation of ions is determined not only via the solvation energy difference of X^- and Y^- but also via the intrinsic surface propensity of X^- and Y^-.

The finding that the intrinsic surface propensity of ions determines the surface enhancement of ions is in line with the observation that such speciation of ions can be seen only when the surface ion population is not saturated. Once the surface ion population is saturated, speciation no longer occurs. This is experimentally confirmed, for example, when the BPh_4^- ion concentration exceeds 10 mM (see Supporting Information), suggesting that the intrinsic surface propensity of ions also matters.

We note that, although the simplified model of ions neglects the impact of the shape of the ions, simulations for SCN^-, SCN^-/Cl^- mixture, and Cl^- solution reveal that ion shape is not a major factor. The data and the discussion are given in the Supporting Information.

Now, we review our results in the context of previous literature. The strong speciation of the charged species has previously been reported for charged surfactants.[31,32,59] Surfactants are amphiphiles containing a hydrophobic part, which prefers to be exposed to the air at the water−air interface. The strong speciation is the result of the hydrophobicity of surfactant molecules as well as the large solvation energy gap between the dissolved salt and the surfactants. Similarly, strong speciation is observed for SCN^- and BPh_4^- anions. These ions are recognized as hydrophobic ions, owing to their relatively low charge density and associated low solvation energy. This hydrophobicity enhances the speciation effect. On the other hand, the speciation is moderate for the

https://doi.org/10.1021/jacs.3c00517
J. Am. Chem. Soc. 2023, 145, 10622−10630

pairs of NaI/NaCl, $NaClO_4$/NaCl, and Na_2SO_4/NaCl. The solvation energy difference between Cl^- and I^-, ClO_4^-, and SO_4^{2-} ions is moderate since these are less hydrophobic than SCN^- and BPh_4^-.

Our experimental data show that co-solvated ions can salt out other ions, and we generalized our finding based on the simple model ions. Our generalization suggests that this speciation occurs not only for the typical ions but also for the charged molecules. In fact, it has been reported that hydrophobic anions such as bromide and iodide and surfactants/lipids tend to appear at the interfaces upon the addition of salt.[26,27,29,31,32,59,60] Some of these pioneering works explain this phenomenon, which may be relevant for Jones−Ray effect, by the charge-neutralization/hydrophobization[31,60] and by the difference in thermodynamic factors such as ion hydration.[26,27,29,30] In line with refs 26 27 29, and 30, our quantitative comparison between HD-SFG data and simulations suggests that this phenomenon can be understood in the framework of the above model: the more hydrophobic anions/surfactants tend to appear at the interface because the hydrophilic ions generated by dissolving salt into water push the hydrophobic anion/surfactant out of the bulk away to the interfaces. The current mechanism can also explain why organic compounds, including volatile organo-iodine compounds, are contained in a sea spray with a high concentration.[61,62]

In summary, we have examined the ion composition at the water−air interface in the presence of pairs of co-solvated ions using HD-SFG and TR-SFG. HD-SFG spectra show that more hydrophobic (hydrophilic) ion tends to be salted out (in). The HD-SFG spectra reveal the tendency of the speciation of ions following the Hofmeister series, and the enhanced surface propensity of the hydrophobic ions are compensated by the hydrophilic ions. The amount of the enhanced surface propensity of the hydrophobic anions due to the presence of the hydrophilic anions is at most 50% among the anions considered in the Hofmeister series. The model simulation indicated that the extent of the speciation is governed by two factors: the solvation energy gap between the ions and the hydrophobicity of the ions. When the solvation energy gap is larger, the speciation is more apparent. The speciation is further enhanced for more hydrophobic ions. This mechanism, corroborated by the quantitative agreement between HD-SFG data and simulations, provides a unified, quantitative view of the speciation of ions and the enhanced surface propensity of the surfactant/lipid in the presence of ions.

MATERIALS AND METHODS

Sample Preparation. Sodium iodide (>99.5%) was purchased from Alfa Aesar. Sodium thiocyanate (99.99%), sodium tetraphenyl borate (99.5%), and D_2O (>99.9%) were obtained from Sigma-Aldrich for the HD-SFG measurements. For the TR-SFG experiments, D_2O (99.9%) was obtained by Eurisotop, and HCl (37%) was obtained from VWR. Sodium perchlorate, anhydrous (>98%), was obtained from Thermo Scientific. Sodium chloride (≥99.5%) and sodium sulfate (≥99%) were purchased from Carl Roth GmbH. Sodium chloride was baked at 500 °C for 8 h before use. Other materials were used as received. The DCl solution was prepared by mixing the HCl solution into D_2O. To avoid the oxidation of iodide ions and BPh_4^- ions, we dissolved the sodium iodide salt into D_2O under N_2 atmosphere and in a dark room just before SFG experiments.

HD-SFG Measurement. We used a collinear beam geometry using a Ti/sapphire regenerative amplifier (Spitfire Ace, Spectra-Physics, centered at 800 nm, ∼40 fs pulse duration, 5 mJ pulse energy, 1 kHz repetition rate). A part of the output was used to generate a broadband IR pulse in an optical parametric amplifier (Light Conversion TOPAS-C) with a silver gallium disulfide ($AgGaS_2$) crystal. The other part of the output was directed through a pulse shaper consisting of a grating-cylindrical mirror system to generate a narrowband visible pulse with a bandwidth of ∼10 cm^{-1}. The IR and visible beams were first focused on a 20 μm thick y-cut quartz plate to generate an LO signal. Then, these beams were collinearly passed through a 5 mm thick STO plate for the phase modulation and were focused on the sample surface at angles of incidence of 45° for visible and IR pulses, respectively. The SFG signal from the sample interfered with the SFG signal from the LO, generating the SFG interferogram. The SFG interferogram was dispersed in a spectrometer and detected by a liquid-nitrogen cooled CCD camera. The complex-valued second-order nonlinear susceptibility ($\chi^{(2)}$) from the samples were obtained via the Fourier analysis of the interferogram and normalization by that from a z-cut quartz crystal. The measurements were performed with the ssp (denoting s-, s-, and p-polarized SFG, visible, and IR beams, respectively) polarization combination. Using D_2O rather than H_2O provides us with improved sensitivity since the measurements are not complicated by water vapor. We expect the conclusions drawn here for D_2O to also be valid for H_2O.

TR-SFG Measurement. The details of the TR-SFG setup are noted elsewhere.[63] In short, we used the homodyne detection with a Ti/sapphire regenerative amplifier (Spitfire Ace, Spectra-Physics, centered at 800 nm, ∼40 fs pulse duration, 10 mJ pulse energy, 1 kHz repetition rate). The SFG signal was guided into a spectrometer and was detected using an Andor Newton EMCCD camera. The IR pump beam was centered at 2500 cm^{-1}. To record pump−probe spectra, a chopper blocks every second laser pulse in the pump laser path, and a vibrating mirror separates the pumped and unpumped signal spatially on the CCD camera. We obtained the time evolution of integrated SFG intensities ($I(t)$) in the range from 2300 to 2400 cm^{-1}. The details of the analysis can be found in the Supporting Information.

MD Simulation for the Aqueous Solution. We performed the force field MD simulation for the aqueous solution systems with two anion species and a single cation species. The two anion species have different Lennard−Jones (LJ) radii. We used the 25 Å × 25 Å × 150 Å simulation cell, where we contained 1000 water molecules, 40 cations, and 20 anions with a larger LJ radius (X^- ion) and 20 anions with a smaller LJ radius (Y^- ion). We used the TIP4P/2005 model for the H_2O molecules[64] and the force field models of Na^+ for cations,[56] while for X^- and Y^-, we used the LJ radii (σ_{X^-}), which were the LJ radius for the force field model of Cl^- (σ_{cl^-}) multiplied by the scale factors. For the SCN^- force field, we obtained the parameters from ref 65. To constrain the geometry of the water model, we used LINCS.[66] For describing ion−ion and ion−water interactions, we used the mixing rule based on the Lorentz−Berthelot rules. We used a cut-off distance of 11 Å for van der Waals interactions and the 3D Ewald summation, smooth particle mesh Ewald,[67] without a specific dipole correction scheme for taking into account the long-range electrostatics. Note that although the simulation and experiment used H_2O and D_2O, respectively, the nuclear quantum effects on the speciation of ions are negligible (see Supporting Information).

We prepared the system which has the same LJ radius of the initial configuration generated by using the PACKMOL software.[68] MD simulations were performed by using the GROMACS software.[69] We used a 2 fs time step for integrating equations of motion. We ran the total 200 ns MD simulation in the NVT ensemble and used the first 20 ns for the equilibration. The target temperature was 300 K, controlled via canonical sampling through the velocity rescaling method.[70] The time constant for the thermostat was 1 ps. The trajectories were sampled every 20 ps.

ASSOCIATED CONTENT

Supporting Information

The Supporting Information is available free of charge at https://pubs.acs.org/doi/10.1021/jacs.3c00517.

https://doi.org/10.1021/jacs.3c00517
J. Am. Chem. Soc. 2023, 145, 10622−10630

Sample preparation, details of HD- and TR-SFG measurements, refractive index of the electrolyte solution, analysis of the TR-SFG data, nuclear quantum effects on the ions' speciation, effect of the ions' interfacial concentrations on the ions' speciation, details of the calculation of solvation energy, depth profiles of ions at the water−vapor interfaces, and surface tension measurement (PDF)

AUTHOR INFORMATION

Corresponding Authors

Mischa Bonn − *Max Planck Institute for Polymer Research, Mainz 55128, Germany;* orcid.org/0000-0001-6851-8453; Email: bonn@mpip-mainz.mpg.de

Yuki Nagata − *Max Planck Institute for Polymer Research, Mainz 55128, Germany;* orcid.org/0000-0001-9727-6641; Email: nagata@mpip-mainz.mpg.de

Authors

Takakazu Seki − *Max Planck Institute for Polymer Research, Mainz 55128, Germany; Graduate School of Science and Technology, Hirosaki University, Hirosaki 036-8561 Aomori, Japan;* orcid.org/0000-0002-3999-2313

Chun-Chieh Yu − *Max Planck Institute for Polymer Research, Mainz 55128, Germany*

Kuo-Yang Chiang − *Max Planck Institute for Polymer Research, Mainz 55128, Germany;* orcid.org/0000-0001-5446-0270

Alessandro Greco − *Max Planck Institute for Polymer Research, Mainz 55128, Germany*

Xiaoqing Yu − *Max Planck Institute for Polymer Research, Mainz 55128, Germany*

Fumiki Matsumura − *Max Planck Institute for Polymer Research, Mainz 55128, Germany*

Complete contact information is available at: https://pubs.acs.org/10.1021/jacs.3c00517

Author Contributions

#T.S. and C.-C.Y. contributed equally.

Funding

Open access funded by Max Planck Society.

Notes

The authors declare no competing financial interest.

Correspondence and requests for materials should be addressed to M.B. and Y.N.

All data needed to evaluate the conclusions in the paper are present in the paper and the Supporting Information. Additional data related to this paper may be requested from the authors.

ACKNOWLEDGMENTS

We thank Johannes Hunger and Sho Imoto for a fruitful discussion. We are grateful for the financial support from the MaxWater initiative of the Max Planck Society. T.S. was supported by the Kurita Water and Environment Foundation (22E005) and by the Sumitomo Foundation (2200651). A.G. acknowledges the financial support from European Union's Horizon 2020 research and innovation program under the Marie Skłodowska-Curie grant agreement no. 811284 (UHMob). X.Y. thanks the support of China Scholarship Council.

REFERENCES

(1) George, I. J.; Abbatt, J. P. D. Heterogeneous Oxidation of Atmospheric Aerosol Particles by Gas-Phase Radicals. *Nat. Chem.* **2010**, *2*, 713−722.

(2) Carpenter, L. J.; MacDonald, S. M.; Shaw, M. D.; Kumar, R.; Saunders, R. W.; Parthipan, R.; Wilson, J.; Plane, J. M. C. Atmospheric Iodine Levels Influenced by Sea Surface Emissions of Inorganic Iodine. *Nat. Geosci.* **2013**, *6*, 108−111.

(3) Seki, T.; Yu, X.; Zhang, P.; Yu, C.-C.; Liu, K.; Gunkel, L.; Dong, R.; Nagata, Y.; Feng, X.; Bonn, M. Real-Time Study of on-Water Chemistry: Surfactant Monolayer-Assisted Growth of a Crystalline Quasi-2D Polymer. *Chem* **2021**, *7*, 2758−2770.

(4) Kusaka, R.; Nihonyanagi, S.; Tahara, T. The Photochemical Reaction of Phenol Becomes Ultrafast at the Air−Water Interface. *Nat. Chem.* **2021**, *13*, 306−311.

(5) Chiang, K. Y.; Seki, T.; Yu, C. C.; Ohto, T.; Hunger, J.; Bonn, M.; Nagata, Y. The Dielectric Function Profile across the Water Interface through Surface-Specific Vibrational Spectroscopy and Simulations. *Proc. Natl. Acad. Sci. U.S.A.* **2022**, *119*, No. e2204156119.

(6) Jungwirth, P.; Tobias, D. J. Specific Ion Effects at the Air/Water Interface. *Chem. Rev.* **2006**, *106*, 1259−1281.

(7) Brown, M. A.; D'Auria, R.; Kuo, I.-F. W.; Krisch, M. J.; Starr, D. E.; Bluhm, H.; Tobias, D. J.; Hemminger, J. C. Ion Spatial Distributions at the Liquid−Vapor Interface of Aqueous Potassium Fluoride Solutions. *Phys. Chem. Chem. Phys.* **2008**, *10*, 4778−4784.

(8) Chang, T.-M.; Dang, L. X. Recent Advances in Molecular Simulations of Ion Solvation at Liquid Interfaces. *Chem. Rev.* **2006**, *106*, 1305−1322.

(9) Brown, E. C.; Mucha, M.; Jungwirth, P.; Tobias, D. J. Structure and Vibrational Spectroscopy of Salt Water/Air Interfaces: Predictions from Classical Molecular Dynamics Simulations. *J. Phys. Chem. B* **2005**, *109*, 7934−7940.

(10) Ishiyama, T.; Morita, A. Molecular Dynamics Study of Gas-Liquid Aqueous Sodium Halide Interfaces. I. Flexible and Polarizable Molecular Modeling and Interfacial Properties. *J. Phys. Chem. C* **2007**, *111*, 721−737.

(11) Yagasaki, T.; Saito, S.; Ohmine, I. Effects of Nonadditive Interactions on Ion Solvation at the Water/Vapor Interface: A Molecular Dynamics Study. *J. Phys. Chem. A* **2010**, *114*, 12573−12584.

(12) Caleman, C.; Hub, J. S.; van Maaren, P. J.; van der Spoel, D. Atomistic Simulation of Ion Solvation in Water Explains Surface Preference of Halides. *Proc. Natl. Acad. Sci. U.S.A.* **2011**, *108*, 6838−6842.

(13) Piatkowski, L.; Zhang, Z.; Backus, E. H. G.; Bakker, H. J.; Bonn, M. Extreme Surface Propensity of Halide Ions in Water. *Nat. Commun.* **2014**, *5*, 4083.

(14) Allen, H. C.; Casillas-Ituarte, N. N.; Sierra-Hernández, M. R.; Chen, X.; Tang, C. Y. Shedding Light on Water Structure at Air-Aqueous Interfaces: Ions, Lipids, and Hydration. *Phys. Chem. Chem. Phys.* **2009**, *11*, 5538−5549.

(15) Petersen, P. B.; Johnson, J. C.; Knutsen, K. P.; Saykally, R. J. Direct Experimental Validation of the Jones−Ray Effect. *Chem. Phys. Lett.* **2004**, *397*, 46−50.

(16) Ji, N.; Ostroverkhov, V.; Tian, C. S.; Shen, Y. R. Characterization of Vibrational Resonances of Water-Vapor Interfaces by Phase-Sensitive Sum-Frequency Spectroscopy. *Phys. Rev. Lett.* **2008**, *100*, 096102.

(17) Sthoer, A. P. A.; Tyrode, E. C. Anion Specific Effects at Negatively Charged Interfaces: Influence of Cl^-, Br^-, I^-, and SCN^- on the Interactions of Na^+ with the Carboxylic Acid Moiety. *J. Phys. Chem. B* **2021**, *125*, 12384−12391.

(18) Ghosal, S.; Hemminger, J. C.; Bluhm, H.; Mun, B. S.; Hebenstreit, E. L. D.; Ketteler, G.; Ogletree, D. F.; Requejo, F. G.; Salmeron, M. Electron Spectroscopy of Aqueous Solution Interfaces Reveals Surface Enhancement of Halides. *Science* **2005**, *307*, 563−566.

(19) Hiranuma, Y.; Kaniwa, K.; Shoji, M.; Mafuné, F. Solvation Structures of Iodide on and below a Surface of Aqueous Solution

Studied by Photodetachment Spectroscopy. *J. Phys. Chem. A* **2011**, *115*, 8493−8497.
(20) Enami, S.; Mishra, H.; Hoffmann, M. R.; Colussi, A. J. Hofmeister Effects in Micromolar Electrolyte Solutions. *J. Chem. Phys.* **2012**, *136*, 154707.
(21) Prather, K. A.; Bertram, T. H.; Grassian, V. H.; Deane, G. B.; Stokes, M. D.; DeMott, P. J.; Aluwihare, L. I.; Palenik, B. P.; Azam, F.; Seinfeld, J. H.; Moffet, R. C.; Molina, M. J.; Cappa, C. D.; Geiger, F. M.; Roberts, G. C.; et al. Bringing the Ocean into the Laboratory to Probe the Chemical Complexity of Sea Spray Aerosol. *Proc. Natl. Acad. Sci. U.S.A.* **2013**, *110*, 7550−7555.
(22) Rogers, M. M.; Neal, J. F.; Saha, A.; Algarni, A. S.; Hill, T. C. J.; Allen, H. C. The Ocean's Elevator: Evolution of the Air−Seawater Interface during a Small-Scale Algal Bloom. *ACS Earth Space Chem.* **2020**, *4*, 2347−2357.
(23) Björneholm, O.; Hansen, M. H.; Hodgson, A.; Liu, L. M.; Limmer, D. T.; Michaelides, A.; Pedevilla, P.; Rossmeisl, J.; Shen, H.; Tocci, G.; Tyrode, E.; Walz, M. M.; Werner, J.; Bluhm, H. Water at Interfaces. *Chem. Rev.* **2016**, *116*, 7698−7726.
(24) Chance, R. J.; Tinel, L.; Sherwen, T.; Baker, A. R.; Bell, T.; Brindle, J.; Campos, M. L. A. M.; Croot, P.; Ducklow, H.; Peng, H.; Hopkins, F.; Hoogakker, B.; Hughes, C.; Jickells, T. D.; Loades, D.; et al. Global Sea-Surface Iodide Observations, 1967−2018. *Sci. Data* **2019**, *6*, 286.
(25) Zdrali, E.; Baer, M. D.; Okur, H. I.; Mundy, C. J.; Roke, S. The Diverse Nature of Ion Speciation at the Nanoscale Hydrophobic/Water Interface. *J. Phys. Chem. B* **2019**, *123*, 2414−2423.
(26) Bruce, E. E.; Bui, P. T.; Rogers, B. A.; Cremer, P. S.; van derVegt, N. F. A. Nonadditive Ion Effects Drive Both Collapse and Swelling of Thermoresponsive Polymers in Water. *J. Am. Chem. Soc.* **2019**, *141*, 6609−6616.
(27) Bui, P. T.; Cremer, P. S. Cation Identity Affects Nonadditivity in Salt Mixtures Containing Iodide and Sulfate. *J. Solution Chem.* **2021**, *50*, 1443−1456.
(28) Lee, S. S.; Park, C.; Sturchio, N. C.; Fenter, P. Nonclassical Behavior in Competitive Ion Adsorption at a Charged Solid-Water Interface. *J. Phys. Chem. Lett.* **2020**, *11*, 4029−4035.
(29) Ottosson, N.; Heyda, J.; Wernersson, E.; Pokapanich, W.; Svensson, S.; Winter, B.; Öhrwall, G.; Jungwirth, P.; Björneholm, O. The Influence of Concentration on the Molecular Surface Structure of Simple and Mixed Aqueous Electrolytes. *Phys. Chem. Chem. Phys.* **2010**, *12*, 10693−10700.
(30) Zhao, Y.; Bharadwaj, S.; van der Vegt, N. F. A. Nonadditive Ion Effects on the Coil−Globule Equilibrium of PNIPAM: A Computer Simulation Study. *Phys. Chem. Chem. Phys.* **2022**, *24*, 10346−10355.
(31) Nguyen, C. V.; Peng, M.; Duignan, T. T.; Nguyen, A. V. Salting-Up of Surfactants at the Surface of Saline Water as Detected by Tensiometry and SFG and Supported by Molecular Dynamics Simulation. *J. Phys. Chem. B* **2022**, *126*, 1063−1075.
(32) Qazi, M. J.; Schlegel, S. J.; Backus, E. H. G.; Bonn, M.; Bonn, D.; Shahidzadeh, N. Dynamic Surface Tension of Surfactants in the Presence of High Salt Concentrations. *Langmuir* **2020**, *36*, 7956−7964.
(33) Ahmed, M.; Nihonyanagi, S.; Kundu, A.; Yamaguchi, S.; Tahara, T. Resolving the Controversy over Dipole versus Quadrupole Mechanism of Bend Vibration of Water in Vibrational Sum Frequency Generation Spectra. *J. Phys. Chem. Lett.* **2020**, *11*, 9123−9130.
(34) Nihonyanagi, S.; Yamaguchi, S.; Tahara, T. Direct Evidence for Orientational Flip-Flop of Water Molecules at Charged Interfaces: A Heterodyne-Detected Vibrational Sum Frequency Generation Study. *J. Chem. Phys.* **2009**, *130*, 204704.
(35) Yamaguchi, S.; Otosu, T. Progress in Phase-Sensitive Sum Frequency Generation Spectroscopy. *Phys. Chem. Chem. Phys.* **2021**, *23*, 18253−18267.
(36) Yu, C.; Seki, T.; Wang, Y.; Bonn, M.; Nagata, Y. Polarization-Dependent Sum-Frequency Generation Spectroscopy for Ångstrom-Scale Depth Profiling of Molecules at Interfaces. *Phys. Rev. Lett.* **2022**, *128*, 226001.
(37) Seki, T.; Yu, C. C.; Chiang, K. Y.; Tan, J.; Sun, S.; Ye, S.; Bonn, M.; Nagata, Y. Disentangling Sum-Frequency Generation Spectra of the Water Bending Mode at Charged Aqueous Interfaces. *J. Phys. Chem. B* **2021**, *125*, 7060−7067.
(38) Ahmed, M.; Nojima, Y.; Nihonyanagi, S.; Yamaguchi, S.; Tahara, T. Comment on "Phase-Sensitive Sum Frequency Vibrational Spectroscopic Study of Air/Water Interfaces: H2O, D2O, and Diluted Isotopic Mixtures" [J. Chem. Phys. 150, 144701 (2019)]. *J. Chem. Phys.* **2020**, *152*, 237101.
(39) Yu, C. C.; Seki, T.; Chiang, K. Y.; Tang, F.; Sun, S.; Bonn, M.; Nagata, Y. Polarization-Dependent Heterodyne-Detected Sum-Frequency Generation Spectroscopy as a Tool to Explore Surface Molecular Orientation and Ångström-Scale Depth Profiling. *J. Phys. Chem. B* **2022**, *126*, 6113−6124.
(40) Stiopkin, I. V.; Weeraman, C.; Pieniazek, P. A.; Shalhout, F. Y.; Skinner, J. L.; Benderskii, A. V. Hydrogen Bonding at the Water Surface Revealed by Isotopic Dilution Spectroscopy. *Nature* **2011**, *474*, 192−195.
(41) Tang, F.; Ohto, T.; Sun, S.; Rouxel, J. R.; Imoto, S.; Backus, E. H. G.; Mukamel, S.; Bonn, M.; Nagata, Y. Molecular Structure and Modeling of Water−Air and Ice−Air Interfaces Monitored by Sum-Frequency Generation. *Chem. Rev.* **2020**, *120*, 3633−3667.
(42) Viswanath, P.; Motschmann, H. Effect of Interfacial Presence of Oriented Thiocyanate on Water Structure. *J. Phys. Chem. C* **2008**, *112*, 2099−2103.
(43) Tian, C.; Byrnes, S. J.; Han, H.-L.; Shen, Y. R. Surface Propensities of Atmospherically Relevant Ions in Salt Solutions Revealed by Phase-Sensitive Sum Frequency Vibrational Spectroscopy. *J. Phys. Chem. Lett.* **2011**, *2*, 1946−1949.
(44) Hua, W.; Verreault, D.; Allen, H. C. Surface Prevalence of Perchlorate Anions at the Air/Aqueous Interface. *J. Phys. Chem. Lett.* **2013**, *4*, 4231−4236.
(45) Nihonyanagi, S.; Kusaka, R.; Inoue, K.-I.; Adhikari, A.; Yamaguchi, S.; Tahara, T. Accurate Determination of Complex $\chi^{(2)}$ Spectrum of the Air/Water Interface. *J. Chem. Phys.* **2015**, *143*, 124707.
(46) Okur, H. I.; Hladílková, J.; Rembert, K. B.; Cho, Y.; Heyda, J.; Dzubiella, J.; Cremer, P. S.; Jungwirth, P. Beyond the Hofmeister Series: Ion-Specific Effects on Proteins and Their Biological Functions. *J. Phys. Chem. B* **2017**, *121*, 1997−2014.
(47) Gregory, K. P.; Elliott, G. R.; Robertson, H.; Kumar, A.; Wanless, E. J.; Webber, G. B.; Craig, V. S. J.; Andersson, G. G.; Page, A. J. Understanding Specific Ion Effects and the Hofmeister Series. *Phys. Chem. Chem. Phys.* **2022**, *24*, 12682−12718.
(48) Jungwirth, P.; Tobias, D. J. Molecular Structure of Salt Solutions: A New View of the Interface with Implications for Heterogeneous Atmospheric Chemistry. *J. Phys. Chem. B* **2001**, *105*, 10468−10472.
(49) Carrier, O.; Backus, E. H. G.; Shahidzadeh, N.; Franz, J.; Wagner, M.; Nagata, Y.; Bonn, M.; Bonn, D. Oppositely Charged Ions at Water−Air and Water−Oil Interfaces: Contrasting the Molecular Picture with Thermodynamics. *J. Phys. Chem. Lett.* **2016**, *7*, 825−830.
(50) Hommel, E. L.; Allen, H. C. The Air−Liquid Interface of Benzene, Toluene, m-Xylene, and Mesitylene: A Sum Frequency, Raman, and Infrared Spectroscopic Study. *Analyst* **2003**, *128*, 750−755.
(51) Chiang, K. Y.; Dalstein, L.; Wen, Y. C. Affinity of Hydrated Protons at Intrinsic Water/Vapor Interface Revealed by Ion-Induced Water Alignment. *J. Phys. Chem. Lett.* **2020**, *11*, 696−701.
(52) Das, S.; Imoto, S.; Sun, S.; Nagata, Y.; Backus, E. H. G.; Bonn, M. Nature of Excess Hydrated Proton at the Water−Air Interface. *J. Am. Chem. Soc.* **2020**, *142*, 945−952.
(53) Hsieh, C.-S.; Bakker, H. J.; Piatkowski, L.; Bonn, M. Gigahertz Modulation of Femtosecond Time-Resolved Surface Sum-Frequency Generation Due to Acoustic Strain Pulses. *J. Phys. Chem. C* **2014**, *118*, 20875−20880.
(54) Xie, W. J.; Gao, Y. Q. A Simple Theory for the Hofmeister Series. *J. Phys. Chem. Lett.* **2013**, *4*, 4247−4252.

(55) Eggimann, B. L.; Siepmann, J. I. Size Effects on the Solvation of Anions at the Aqueous Liquid−Vapor Interface. *J. Phys. Chem. C* **2008**, *112*, 210−218.
(56) Yagasaki, T.; Matsumoto, M.; Tanaka, H. Lennard-Jones Parameters Determined to Reproduce the Solubility of NaCl and KCl in SPC/E, TIP3P, and TIP4P/2005 Water. *J. Chem. Theory Comput.* **2020**, *16*, 2460−2473.
(57) Levin, Y. Polarizable Ions at Interfaces. *Phys. Rev. Lett.* **2009**, *102*, 147803.
(58) Levin, Y.; dosSantos, A. P.; Diehl, A. Ions at the Air-Water Interface: An End to a Hundred-Year-Old Mystery? *Phys. Rev. Lett.* **2009**, *103*, 257802.
(59) Angle, K. J.; Nowak, C. M.; Davasam, A.; Dommer, A. C.; Wauer, N. A.; Amaro, R. E.; Grassian, V. H. Amino Acids Are Driven to the Interface by Salts and Acidic Environments. *J. Phys. Chem. Lett.* **2022**, *13*, 2824−2829.
(60) Duignan, T. T.; Peng, M.; Nguyen, A. V.; Zhao, X. S.; Baer, M. D.; Mundy, C. J. Detecting the Undetectable: The Role of Trace Surfactant in the Jones-Ray Effect. *J. Chem. Phys.* **2018**, *149*, 194702.
(61) Martino, M.; Mills, G. P.; Woeltjen, J.; Liss, P. S. A New Source of Volatile Organoiodine Compounds in Surface Seawater. *Geophys. Res. Lett.* **2009**, *36*, L01609.
(62) Zhdankin, V. V.; Stang, P. J. Chemistry of Polyvalent Iodine. *Chem. Rev.* **2008**, *108*, 5299−5358.
(63) Deiseroth, M.; Bonn, M.; Backus, E. H. G. Orientation Independent Vibrational Dynamics of Lipid-Bound Interfacial Water. *Phys. Chem. Chem. Phys.* **2020**, *22*, 10142−10148.
(64) Abascal, J. L. F.; Vega, C. A General Purpose Model for the Condensed Phases of Water: TIP4P/2005. *J. Chem. Phys.* **2005**, *123*, 234505.
(65) Tesei, G.; Aspelin, V.; Lund, M. Specific Cation Effects on SCN- in Bulk Solution and at the Air-Water Interface. *J. Phys. Chem. B* **2018**, *122*, 5094−5105.
(66) Hess, B.; Bekker, H.; Berendsen, H. J. C.; Fraaije, J. G. E. M. LINCS: A Linear Constraint Solver for Molecular Simulations. *J. Comput. Chem.* **1997**, *18*, 1463−1472.
(67) Essmann, U.; Perera, L.; Berkowitz, M. L.; Darden, T.; Lee, H.; Pedersen, L. G. A Smooth Particle Mesh Ewald Method. *J. Chem. Phys.* **1995**, *103*, 8577−8593.
(68) Martínez, L.; Andrade, R.; Birgin, E. G.; Martínez, J. M. Packmol: A Package for Building Initial Configurations for Molecular Dynamics Simulations. *J. Comput. Chem.* **2009**, *30*, 2157−2164.
(69) Abraham, M. J.; Murtola, T.; Schulz, R.; Páll, S.; Smith, J. C.; Hess, B.; Lindahl, E. GROMACS : High Performance Molecular Simulations through Multi-Level Parallelism from Laptops to Supercomputers. *SoftwareX* **2015**, *1*−*2*, 19−25.
(70) Bussi, G.; Donadio, D.; Parrinello, M. Canonical Sampling through Velocity Rescaling. *J. Chem. Phys.* **2007**, *126*, 014101.

https://doi.org/10.1021/jacs.3c00517
J. Am. Chem. Soc. 2023, 145, 10622−10630